

# Phase Noise in Capacitively Coupled Micromechanical Oscillators

Ville Kaajakari, *Member, IEEE*, Jukka K. Koskinen, and Tomi Mattila, *Member, IEEE*

**Abstract**—Phase noise in capacitively coupled microresonator-based oscillators is investigated. A detailed analysis of noise mixing mechanisms in the resonator is presented, and the capacitive transduction is shown to be the dominant mechanism for low-frequency  $1/f$ -noise mixing into the carrier sidebands. Thus, the capacitively coupled micromechanical resonators are expected to be more prone to the  $1/f$ -noise aliasing than piezoelectrically coupled resonators. The analytical work is complemented with simulations, and a highly efficient and accurate simulation method for a quantitative noise analysis in closed-loop oscillator applications is presented. Measured phase noise for a microresonator-based oscillator is found to agree with the developed analytical and simulated noise models.

## I. INTRODUCTION

MICROMECHANICAL resonators are potentially a compact and economic alternative to the size consuming quartz crystals that are ubiquitous in today's electronic devices. The microresonators have been demonstrated to offer quality factors comparable to crystals ( $Q > 100\,000$  at 10 MHz), but achieving a sufficient power handling capacity with micron-sized components has been a challenge [1]. For silicon resonators, the maximum vibration amplitude, and therefore the power handling capacity, are limited by nonlinearities. Understanding these fundamental nonlinear effects recently has led to the demonstration of microresonator that provides power-handling capacity comparable to macroscopic crystals [2]–[4]. Consequently, a microresonator-based oscillator has been demonstrated to offer noise floor of  $-150$  dBc/Hz at 13 MHz, meeting the typical phase noise requirements for wireless communication [5]. Recently, comparable performance has been obtained with a polycrystalline silicon disk resonator and integrated electronics [6].

As prior work on microresonators has focused on the power-handling capacity, only little attention has been given to near-carrier noise in micro-oscillators, but considerable theoretical and experimental work has been done on phase noise in conventional oscillators [7]–[11]. A significant near-carrier noise source is the aliasing of  $1/f$ -noise to carrier side-bands due to the mixing of low-frequency noise and carrier signal in the active circuit elements. In this paper we show that, in addition to amplifier nonlinearities, the electrostatic transduction commonly used for coupling to silicon resonators is inherently nonlinear

and leads to aliasing of noise. This process is illustrated in Fig. 1 that shows a schematic representation of an oscillator comprised of a resonator and sustaining amplifier. In addition to amplifying oscillation signal  $u_{ac}$ , the amplifier output may present a significant amount of low-frequency  $1/f$ -noise to the resonator input. A linear resonator element would effectively filter out this low-frequency noise, but nonlinearities in the resonator will lead to unwanted aliasing of the low-frequency noise to carrier side-bands. Thus, the capacitive coupling is expected to be intrinsically more prone to noise aliasing than the conventional piezoelectrical coupling.

Section II of this paper reviews the electrostatic actuation of microresonators, and the electrical equivalent is developed. Nonlinear effects are analyzed, and the maximum vibration amplitude is estimated. In Section III, the noise aliasing mechanisms in the resonator are investigated. The aliasing due to the capacitive transduction is compared to mixing due to nonlinear spring effects, and the capacitive transduction is shown to be the dominant noise-mixing mechanism in the resonator. Section IV incorporates the aliased noise into the “Leeson’s” phase noise model. In Section V, a simulation method is demonstrated to accurately analyze complex noise aliasing behavior in nonlinear oscillators, and the analytical model is verified. The theoretical model is compared to experimentally measured phase noise in Section VI and good agreement is found. In Section VII, the implications of the noise aliasing on oscillator design are discussed.

## II. ELECTROSTATICALLY ACTUATED MICRORESONATORS

In this section, a linear electrical model for the resonator is reviewed followed by the analysis of nonlinear forces introduced by the electrostatic coupling.

### A. Linear Resonator Model

The model used in this paper for the microresonator is shown in Fig. 2. The mechanical vibrations are modeled with a lumped mass-spring-dashpot resonator in which the lumped mass and spring are derived from the resonator geometry and mode-shape. The coupling to the resonator is provided by the electrostatic transduction over the narrow gap  $d$ . The equation of motion for forced oscillations of the mass-spring-dashpot system in Fig. 2 is:

$$m\ddot{x} + \gamma\dot{x} + kx = F_e, \quad (1)$$

Manuscript received February 18, 2005; accepted May 26, 2005.

The authors are with VTT Technical Research Centre of Finland, VTT Information Technology, Espoo, Finland (e-mail: ville.kaaajakari@vtt.fi).

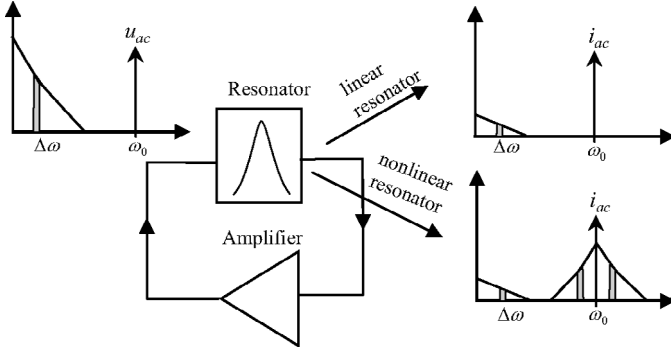


Fig. 1. Schematic representation of noise aliasing in micro-oscillator. A linear resonator would filter out the amplifier low-frequency  $1/f$ -noise present at the resonator input, but nonlinear filtering element will result in noise aliasing.

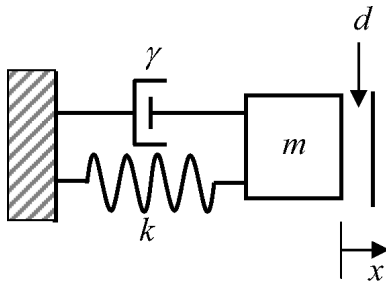


Fig. 2. Mechanical lumped model for the resonator.

where  $m$  is the lumped mass,  $\gamma$  is the damping coefficient,  $F_e$  is the electrostatic forcing term, and  $k$  is the mechanical spring constant. We also define the natural frequency  $\omega_0 = \sqrt{k/m}$  and the quality factor  $Q = \omega_0 m / \gamma$ . The resonator displacement  $x$  due to the force  $F_e$  is given by:

$$x = H(\omega)F_e, \quad (2)$$

where the force-displacement transfer function  $H(\omega)$  from (1) is:

$$H(\omega) = \frac{k^{-1}}{1 - \omega^2/\omega_0^2 + i\omega/Q\omega_0}. \quad (3)$$

The electrostatic force actuating the resonator is:

$$F_e = \frac{1}{2} \frac{\partial C}{\partial x} (U_{dc} + u_{ac})^2, \quad (4)$$

where  $U_{dc}$  is the direct current (DC)-bias voltage over the gap,  $u_{ac}$  is the alternating current (AC)-excitation voltage, and:

$$C = \epsilon_0 \frac{A_{el}}{d - x}, \quad (5)$$

is the transducer working capacitance that depends on the permittivity of free space  $\epsilon_0$ , the electrode area  $A_{el}$ , and the nominal electrode gap  $d$ . The current through the electrode is:

$$i_{sig} = \frac{\partial CU}{\partial t} \approx \frac{\partial C}{\partial t} U_{dc} + C_0 \frac{\partial u_{ac}}{\partial t}, \quad (6)$$

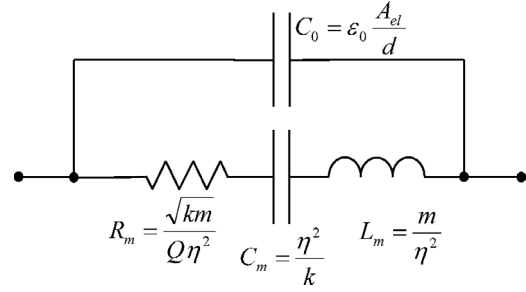


Fig. 3. The electrical equivalent circuit for MEMS-based oscillator.

where  $C_0$  is the capacitance at zero displacement. In (6), the first term is due to the capacitance variations (motional current  $i_m$ ), and the second term is the normal AC-current through the capacitance. The electromechanical transduction factor is identified as [12]:

$$\eta = U_{dc} \frac{\partial C}{\partial x} \approx U_{dc} \frac{C_0}{d}. \quad (7)$$

The resulting relation between the motional current  $i_m$ , the mechanical transducer velocity  $\dot{x}$ , the excitation voltage  $u_{ac}$ , and the force  $F_e$  at the excitation frequency are:

$$\begin{aligned} i_m &\approx \eta \dot{x}, \\ F_e &\approx \eta u_{ac}, \end{aligned} \quad (8)$$

where the displacement  $x$  is assumed to be small compared to the gap  $d$ . By substituting (8) into (1), an electrical equivalent circuit shown in Fig. 3 can be derived. The component values are:

$$\begin{aligned} R_m &= \sqrt{km}/Q\eta^2 = k/\omega_0 Q\eta^2, \\ C_m &= \eta^2/k, \\ L_m &= m/\eta^2, \text{ and} \\ C_0 &= \epsilon_0 A_{el}/d_0. \end{aligned} \quad (9)$$

The important observation is that, to obtain a small motional resistance  $R_m$ , a large electromechanical transduction factor is needed requiring either a small gap  $d$  or a large DC-bias voltage  $U_{dc}$ . In practice, the voltage usually is limited by system considerations and, thus, a small gap, typically less than  $1 \mu\text{m}$ , is needed. Unfortunately, as will be seen in the following sections, the small gap will result in unwanted nonlinear effects that limit the vibration amplitude and cause noise aliasing.

### B. Nonlinear Electrostatic Spring Force

Due to the inverse relationship between the electrode displacement and the parallel plate capacitance, the electrostatic coupling introduces nonlinear spring terms. Additionally, nonlinear effects of mechanical origins are possible, and most fundamentally material nonlinearities set the limit for the miniaturization [4] [13]. In this paper, however, the gap is assumed small, and therefore, the capacitive nonlinearity dominates. Thus, a linear mechanical

model is used, and the accurate nonlinear model is used for the electromechanical transduction [14].

The nonlinear electrostatic spring constants are obtained by a series expansion of the electrostatic force:

$$F = \frac{U_{dc}^2}{2} \frac{\partial C}{\partial x}. \quad (10)$$

Including terms up to the second order gives for the electrostatic spring:

$$k_e(x) = k_{0e}(1 + k_{1e}x + k_{2e}x^2) \\ k_{0e} = -\frac{U_{DC}^2 C_0}{d^2}, \quad k_{1e} = \frac{3}{2d}, \quad \text{and} \quad k_{2e} = \frac{2}{d^2}. \quad (11)$$

The linear electrostatic spring  $k_{0e}$  is negative, and thus lowers the resonance frequency. Of the nonlinear terms, the second-order correction  $k_{2e}$  can be shown to dominate [1].

The electrostatic nonlinearity limits the resonator drive level as at high-vibration amplitudes; the amplitude-frequency curve is not a single valued function and oscillations may even become chaotic [1] [4]. Therefore, the maximum usable vibration amplitude can be estimated from the largest vibration amplitude before a bifurcation. This critical vibration amplitude can be written as [4], [15]:

$$x_c = \frac{2}{\sqrt{3\sqrt{3}Q|\kappa|}}, \quad (12)$$

where:

$$\kappa = \frac{3k_{2e}k_{0e}}{8k} - \frac{5k_{1e}^2 k_{0e}^2}{12k^2}. \quad (13)$$

Defining the drive level as the motional current through the resonator, the maximum drive level is given by (8) and (12) and can be written as:

$$i_m^{\max} = \eta\omega_0 x_c. \quad (14)$$

As will be seen in Section IV, the maximum drive level sets the noise floor obtainable with microresonator-based oscillator.

The analysis in this section assumed that the nonlinearity is due to the capacitive spring effects, but (12) and (13) are valid also for cases in which mechanical nonlinearities dominate. As an example, in the comb drive actuated resonators, the capacitance depends linearly on displacement [16]. In such a case, the nonlinear springs and the maximum vibration amplitude is estimated from mechanical nonlinearities [4].

### III. ALIASING OF NOISE IN MICRORESONATOR

In addition to the nonlinear spring effects, the capacitive coupling results in up- and down-conversion of noise. As seen from the trigonometric identity:

$$2 \cos \Delta\omega t \cdot \cos \omega_0 t = \cos(\omega_0 + \Delta\omega)t + \cos(\omega_0 - \Delta\omega)t, \quad (15)$$

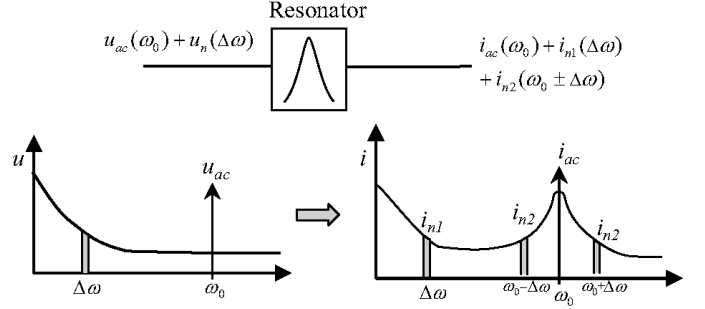


Fig. 4. Schematic representation of noise aliasing. Low-frequency noise  $u_n(\Delta\omega)$  present at filter input is aliased to carrier side-bands  $\omega_0 \pm \Delta\omega$  due to mixing in resonator.

the low-frequency noise signal at  $\Delta\omega$  multiplied with the carrier signal at  $\omega_0$  results in additional near-carrier noise side-bands at  $\omega_0 \pm \Delta\omega$ . As illustrated in Fig. 5, this mixing in the resonator causes aliasing of low-frequency noise to carrier side-bands.

The aliasing of low-frequency noise can be very detrimental to the oscillator phase noise performance as low-frequency  $1/f$ -noise can be considerably larger than the thermal noise floor. The typical low-frequency noise sources present at the resonator input are the active sustaining elements (transistors) in the oscillator circuit that may have a significant amount of  $1/f$ -noise [17]. Resonator biasing also may be noisy, especially if it is implemented with a charge pump. Notably mechanical  $1/f$ -noise also may be significant if the resonator is scaled to nanometer scale [18]. However, the noise up-mixing analysis presented here is not limited to a specific noise source as only the magnitude of the noise at resonator input is needed to predict noise aliasing in the resonator.

In this section, the noise up-mixing due to the electrostatic coupling is analyzed. Mixing due to the electrostatic transduction is compared to mixing due to nonlinear spring effects. As Fig. 4 indicates, the analysis in this section is an open-loop, up-conversion analysis of different up-mixing mechanisms. The closed-loop oscillator analysis, including the effect of positive feedback, is presented in Section IV.

#### A. Mixing Due to Capacitive Current Nonlinearity

Fig. 5(a) illustrates how low-frequency noise  $u_n$  at  $\Delta\omega$  is mixed to a higher frequency due to the time varying gap capacitance. The capacitance is:

$$C(x) \approx C_0 \left(1 + \frac{x_0}{d}\right), \quad (16)$$

where  $x_0$  is the resonator displacement at the excitation frequency. The current through the resonator due to the voltage  $u_n$  is then:

$$i_n = \frac{\partial(C(x)u_n)}{\partial t} \approx \frac{C_0}{d} \dot{x}_0 u_n + C_0 \dot{u}_n. \quad (17)$$

The first term in (17) is responsible for the noise up-conversion and results in noise current at  $\omega_0 \pm \Delta\omega$ . Us-

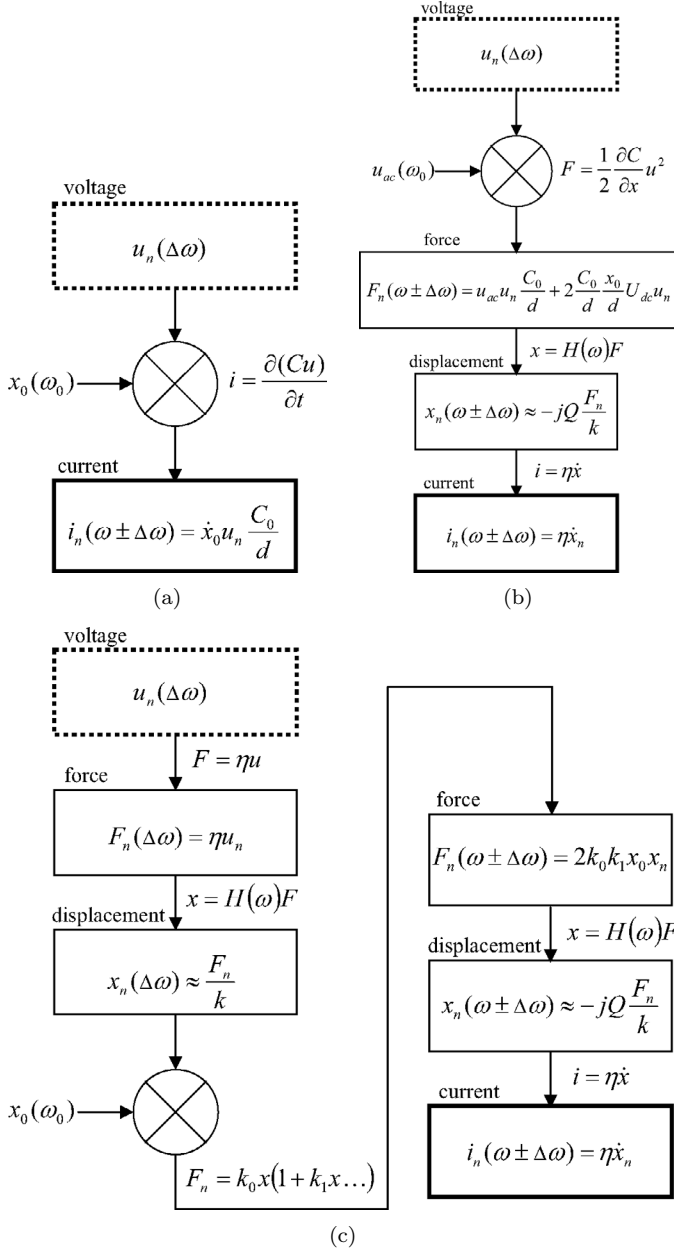


Fig. 5. Different mixing mechanism for the noise voltage  $u_n$  at  $\Delta\omega$  to high-frequency noise current. (a) Time-varying capacitor (plate displacement  $x$ ) results in up-converted noise current. (b) Square force law results in mixing of noise and signal voltages,  $u_n$  and  $u_{ac}$ , respectively. (c) Nonlinear spring force results in mixing of low-frequency and signal frequency vibrations.

ing the relation between the signal voltage and resonator displacement given by (2) and (8), the up-converted noise current due to capacitive current mixing can be written as:

$$i_n^c = 2\Gamma_c u_{ac} u_n, \quad (18)$$

where we have defined the current aliasing factor:

$$\Gamma_c = \frac{Q\omega_0\eta^2}{2kU_{dc}}. \quad (19)$$

As (15) shows, the current  $i_n^c$  given by (18) has equal amplitudes at frequencies  $\omega_0 \pm \Delta\omega$ .

### B. Mixing Due to Capacitive Force Nonlinearity

The second main up-conversion avenue is illustrated in Fig. 5(b). Due to the square force law, the low-frequency noise voltage  $u_n$  at  $\Delta\omega$  is mixed with the high frequency signal voltage  $u_{ac}$  at  $\omega_0$ . The capacitive force is given by:

$$F_n = \frac{U^2}{2} \frac{\partial C}{\partial x} \approx \frac{(U_{dc} + u_{ac} + u_n)^2}{2} \frac{C_0}{d} \left(1 + 2\frac{x_0}{d}\right), \quad (20)$$

where the first three terms of power series expansion of the capacitance have been kept. The products  $u_{ac}u_n$  and  $xu_n$  result in up-converted noise at  $\omega_0 \pm \Delta\omega$ . Thus, the force at  $\omega_0 \pm \Delta\omega$  is:

$$F_n(\omega_0 \pm \Delta\omega) \approx \frac{C_0}{d} u_{ac} u_n + 2\frac{C_0}{d} \frac{x_0}{d} U_{dc} u_n. \quad (21)$$

This high-frequency noise force near the resonator resonance excites the resonator, and the displacement is given by (3). Close to the resonance, the noise-induced displacement is:

$$x_n^F \approx -jQ \frac{F_n}{k}, \quad (22)$$

and the resulting noise current is:

$$i_n^F = \eta \dot{x}_n = -j\eta\omega_0 x_n. \quad (23)$$

Substituting (21) and (22) to (23) and using  $x_0 = -jQ\eta u_{ac}/k$  leads to:

$$i_n^F = 2\Gamma_F u_{ac} u_n, \quad (24)$$

where we have defined the force aliasing factor:

$$\Gamma_F \approx \frac{Q\omega_0\eta^2}{2kU_{dc}} \left(1 - j2\frac{Q\eta U_{dc}}{kd}\right). \quad (25)$$

Here the first term in brackets is due to the square force law [product  $u_{ac}u_n$  in (20)], and the second term in brackets is due to the nonlinear capacitance [product  $xu_n$  in (20)]. If we had kept only the first term of the power series expansion of capacitance [linear capacitance,  $C(x) = C_0(1 + x/d)$ ], then the force aliasing factor would be:

$$\Gamma_F \approx \frac{Q\omega_0\eta^2}{2kU_{dc}} \text{ (linear C)}, \quad (26)$$

which is the same as the current aliasing factor given by (19).

It is of interest to compare the two terms in brackets in (25). Substituting typical microresonator parameters (Table I) gives  $(2Q\eta U_{dc}/kd) \approx 63$ . Thus, the second term in brackets in (25) is the dominant term and the noise aliasing could be significantly reduced with a linear coupling capacitor.

TABLE I  
RESONATOR CHARACTERISTICS AT  $U_{dc} = 20$  V.

Parameter	Symbol	Value	Units
Resonance frequency	$f_0$	13.2	[MHz]
Effective spring constant	$k$	16.8	[MN/m]
Effective mass	$m$	2.44	[nkg]
Quality factor	$Q$	100,000	
Electrode area	$A_{el}$	12,000	$[\mu\text{m}^2]$
Transducer gap	$d$	0.2	$[\mu\text{m}]$
Motional capacitance	$C_m$	168	[aF]
Motional inductance	$L_m$	867	[mH]
Motional resistance	$R_m$	718	$[\Omega]$
Critical amplitude	$x_c$	36.0	[nm]

### C. Mixing Due to Nonlinear Spring Force

The up-conversion avenue due to nonlinear spring force is illustrated in Fig. 5(c). The force due to the noise voltage  $F_n = \eta u_n$  results in low-frequency resonator vibrations. Because these vibrations are far from the resonance, the amplitude is given by:

$$x_n = H(\omega)F_n \approx \frac{\eta u_n}{k}. \quad (27)$$

Due to the nonlinear spring effects, these low-frequency vibrations are multiplied with the vibrations at the signal frequency. Assuming spring force  $F = k_0x(1 + k_1x)$  and substituting  $x = x_0 + x_n$ , the up-converted noise force is:

$$F_n^k = 2k_0k_1x_0x_n. \quad (28)$$

The resulting current can be evaluated as in Section III-B. Assuming that the nonlinear spring is dominated by the capacitive effects given by (11), the up-converted noise current due to nonlinear spring mixing is given by:

$$i_n^k = 2\Gamma_k u_{ac} u_n, \quad (29)$$

where we have defined the spring aliasing factor:

$$\Gamma_k = j \frac{3Q^2 \omega_0 \eta^4 U_{dc}}{2d^2 k^3}. \quad (30)$$

### D. Comparison of Mixing Mechanisms

The ratio of aliasing factors due to the current up-conversion and nonlinear spring mixing given by (19) and (30), respectively, is:

$$\left| \frac{\Gamma_c}{\Gamma_k} \right| = \frac{1}{3Q} \left( \frac{dk}{\eta U_{DC}} \right)^2. \quad (31)$$

Substituting typical microresonator parameters (Table I) into (31) gives  $|\Gamma_c/\Gamma_k| \approx 500$ . Thus, we can conclude that the main aliasing mechanism is the nonlinear electrostatic transduction (capacitive current and force nonlinearity) and not the nonlinear spring effects.

For a linear capacitance  $C(x) = C_0(1 + x/d)$ , the aliasing factors for the current and force up-conversions given

by (19) and (26), respectively, are equal. Substituting typical microresonator parameters (Table I) into (31) gives  $|\Gamma_c| = |\Gamma_F| = 34.8 \mu\text{A}/\text{V}^2$  (linear C). With the inclusion of the nonlinear terms in capacitance, the force aliasing factor given by (25) is  $|\Gamma_F| = 2.2 \text{mA}/\text{V}^2$ . As noted before, this is 63 times larger than for a linear capacitance. Thus, for a parallel plate coupling capacitor, the force up-mixing is the dominant aliasing path.

### E. Simulation of Noise Aliasing

To verify the analytical results, the aliasing of a low-frequency signal was simulated with a harmonic balance circuit simulator [14]. The resonator was excited using a high-frequency signal at the resonance frequency and a small-frequency signal at frequency  $\Delta f$ . Fig. 6(a) shows the simulated aliasing factors  $\Gamma$  at different frequencies  $\Delta f$  obtained using the accurate model with all capacitive nonlinearities included [14]. At small-frequency offsets ( $\Delta f < f_0/2Q$ ) the magnitude of aliasing factor is very close to the analytical estimate of  $|\Gamma| = 2.2 \text{mA}/\text{V}^2$  given by:

$$\Gamma = \Gamma_F + \Gamma_c, \quad (32)$$

where  $\Gamma_F$  and  $\Gamma_c$  are given by (25) and (19), respectively. Outside the resonator bandwidth ( $\Delta f > f_0/2Q$ ), the aliasing is significantly reduced as the motion is not enhanced by the resonator quality factor.

For a linear capacitor, the aliasing shown in Fig. 6(b) is smaller by a factor of 63. Again, the result is close to the analytical result of  $\Gamma = 69.6 \mu\text{A}/\text{V}^2$  given by the sum of (19) and (26). Figs. 6(c) and (d) show the aliasing with only the force and current nonlinearity included in the model, respectively. It is shown that, for small-frequency offsets ( $\Delta f < f_0/2Q$ ), both effects are equal and agree with (19) and (26). At higher offsets, the effect of force nonlinearity is reduced as the resonator is not excited far from the resonance. The aliasing due to current nonlinearity does not show this effect as it is due to direct modulation of the capacitance.

To further validate the noise aliasing analysis, the aliasing factors were simulated at different noise levels. The aliasing factors remained unchanged to noise voltages less than 10 mV. At higher noise levels, the oscillation frequency was changed as the noise started to be significant in comparison to bias voltage. As the typical noise levels are less than  $1 \mu\text{V}/\sqrt{\text{Hz}}$ , the first-order mixing analysis is enough for accurate estimation of noise aliasing in the resonator.

## IV. ANALYTICAL PHASE NOISE MODEL

Here an analytical model for the noise in a closed-loop micromechanical oscillator is developed. The model is based on well-known Leeson's model for the phase noise [7] [8] [10] and is expanded to incorporate the  $1/f$ -noise aliasing in microresonators.

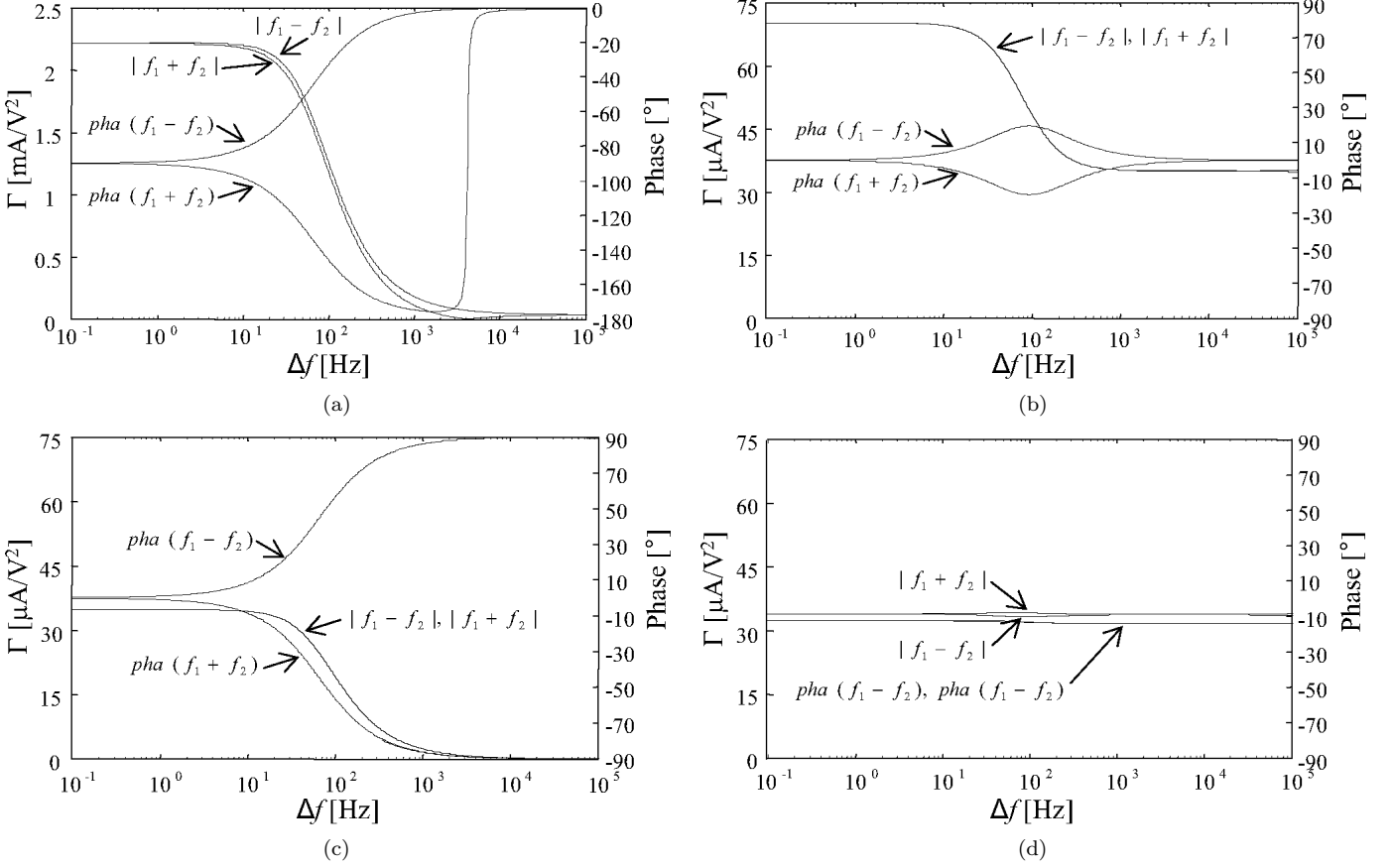


Fig. 6. Aliasing of low-frequency signal due to mixing in capacitive coupling. The resonator is excited with a high-frequency signal at resonance. The low-frequency signal at frequency  $\Delta f$  is mixed to  $f_0 \pm \Delta f$ . The magnitude and relative phase of aliasing factor  $\Gamma$  depends on the nonlinearities included in the model. (a) Accurate nonlinear model ( $C(x) = \epsilon A/(d-x)$ ). (b) Nonlinear current and force model with linear capacitance ( $C(x) = C_0(1 + x/d)$ ). (c) Nonlinear force ( $F \sim U^2$ ) and linear current ( $i \sim \dot{x}$ ) with linear capacitance ( $C(x) = C_0(1 + x/d)$ ). (d) Linear force ( $F \sim u_{ac}$ ) and nonlinear current ( $i \sim \dot{x}U$ ) with linear capacitance ( $C(x) = C_0(1 + x/d)$ ).

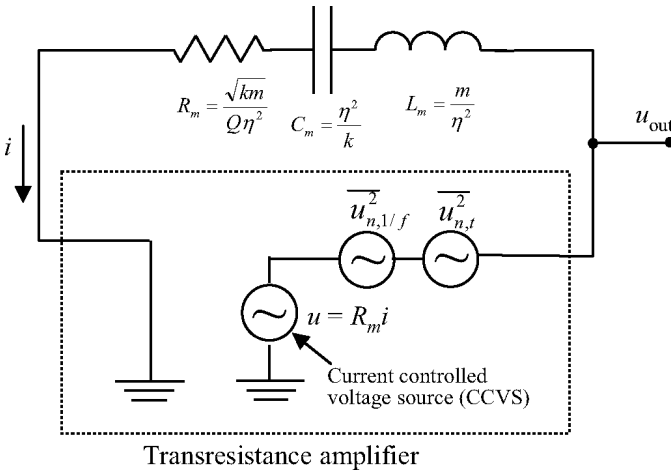


Fig. 7. Idealized oscillator showing ideal resonator and loop amplifier that is DC-coupled to the resonator. The noise sources are associated to the amplifier, but they may well include other noise sources. The total noise at the resonator input is a sum of thermal  $u_{n,t}$  and  $1/f$ -noise  $u_{n,1/f}$ .

Fig. 7 shows an idealized oscillator model. The oscillator circuit is based on a microresonator (modeled using the RLC circuit developed in Section II-A), and a transresistance amplifier ( $u = R_m i$ ) that provides the positive feedback to sustain the oscillations. At resonance,  $L_m$  and  $C_m$  cancel and the amplifier cancels the resistive losses due to  $R_m$ . Thus, the loop gain is unity, and stable oscillations are sustained. The signal voltage at the resonance frequency is denoted  $u_{ac}$ . For this idealized model using a linear amplifier, the amplitude of signal  $u_{ac}$  is arbitrary. In practice it is set by the gain saturation of the loop amplifier. Also, because a linear amplifier is assumed in the analysis, the noise mixing in the amplifier is not included in the model.

Two noise sources are included: thermal noise  $u_{n,t}$  and  $1/f$ -noise  $|u_{n,1/f}|^2 = |u_{n,t}|^2 \omega_c / \Delta\omega$ , where the  $\omega_c$  is the corner frequency for the  $1/f$ -noise. The noise originating from the mechanical dissipation  $R_m$  is omitted as it can be included in the thermal noise  $u_{n,t}$ . For the off-resonance noise analysis, we write the relationship between the output voltage  $u_{out}$  (voltage over the resonator) and the resonator current  $i$  as:

$$i = \frac{u_{out}}{Z} \approx \frac{u_{out}}{R_m + j2\Delta\omega L_m}. \quad (33)$$

Including only the thermal noise source  $u_{n,t}$  and substituting  $u_{out} = u + u_{n,t}$  and  $u = R_m i$  into (33) gives:

$$\frac{u}{R_m} \approx \frac{u + u_{n,t}}{R_m + j2\Delta\omega L_m}. \quad (34)$$

Solving (34) for  $u$  allows writing the noise at the output as:

$$|u_{out}^{n,t}|^2 = |u_{n,t}|^2 \left[ \left( \frac{\omega_0}{2\Delta\omega Q} \right)^2 + 1 \right]. \quad (35)$$

This is the single side-band noise. As the thermal noise in both side bands can be assumed uncorrelated, the dual side-band noise is obtained by multiplying (35) by two.

The  $1/f$ -noise is analyzed as follows: The low-frequency noise voltage  $u_{n,1/f}$  is up-converted in the resonator to noise current given by  $i_{n,1/f} = 2\Gamma u_{ac} u_{n,1/f}$ . This up-converted noise current is picked up by the amplifier and amplified in the feed-back loop. Analysis identical to thermal noise leads to noise voltage at the output given by:

$$|u_{out}^{n,1/f}|^2 = |\Gamma|^2 R_m^2 |u_{ac}|^2 |u_{n,1/f}|^2 \left( \frac{\omega_0}{2\Delta\omega Q} \right)^2. \quad (36)$$

This is the single side-band noise. As noise on both side bands originate from the same  $1/f$ -noise source, they are correlated, and the dual side-band noise is obtained by multiplying (36) by four. Combining (35) and (36), substituting  $|u_{n,1/f}|^2 = |u_{n,t}|^2 \omega_c / \Delta\omega$ , dividing the result by two to account the phase and not the amplitude noise, and normalizing with the signal  $u_{ac}$  gives so-called ‘‘Leeson’s equation’’ for dual side-band phase noise:

$$S_\phi = \frac{|u_{n,t}|^2}{|u_{ac}|^2} \left[ \left( \frac{\omega_0}{2Q\Delta\omega} \right)^2 \left( 1 + 2|\Gamma|^2 R_m^2 |u_{ac}|^2 \frac{\omega_c}{\Delta\omega} \right) + 1 \right]. \quad (37)$$

Eq. (37) gives three regions of operation. Very close to the carrier the phase noise falls as  $1/f^3$  due to the aliased  $1/f$ -noise. This noise cannot be reduced by increasing the vibration amplitude as the noise aliasing is proportional to  $u_{ac}$ . The  $1/f^3$ -region is followed by  $1/f^2$ -region in which thermal noise shaped by the positive feedback dominates. A constant noise floor is seen. Phase noise in the  $1/f^2$ -region and the noise floor can be lowered by increasing the signal voltage  $u_{ac}$ . The minimum obtainable noise floor is limited by the maximum resonator vibration amplitude  $x_c$  given by (12), and the maximum signal voltage can be written as  $u_{ac}^{MAX} = x_c k / Q\eta$ .

In the region in which  $1/f$ -noise dominates, (37) can be written as:

$$S_\phi = \frac{\omega_0^2 |\Gamma|^2 R_m^2 \omega_c}{2Q^2 \Delta\omega^3} |u_{n,t}|^2. \quad (38)$$

As the near-carrier noise in microresonators is often dominated by  $1/f$ -noise, (38) can be used for a quick estimation of the obtainable phase noise performance.

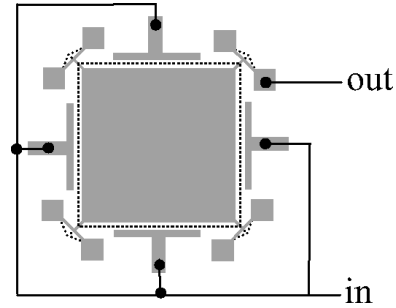


Fig. 8. Schematic of the square extensional mode microresonator showing the mode in extended shape [2] [5].

## V. SIMULATION OF THE PHASE NOISE

To verify the analytical noise model, the large-signal-small-signal (LSSS) method that has been implemented in a commercial circuit simulation software is used for the oscillator noise analysis [19]. The large signal oscillator operation point is obtained with the large signal harmonic balance (HB) analysis. After the HB analysis, a small signal noise analysis is carried out using the time varying operation point. The noise signal is assumed to be sufficiently small as not to affect the oscillator operation point. Furthermore, only mixing products involving the large signals are accounted and noise-noise products are neglected. As noise is much smaller than the carrier, the noise-noise mixing products are small, and this approximation is justified.

The oscillator circuit consists of two components shown in Fig. 7: the resonator and the sustaining amplifier. As discussed in Section II, the mechanical part of the resonator is modeled as a lumped mass-spring-dashpot system. For electromechanical coupling, accurate nonlinear model of the parallel plate capacitor is used [14]. The resonator chosen for the simulation is based on published values for an extensional mode plate resonator [2] [5]. The resonator is schematically shown in Fig. 8, and its properties are summarized in Table I. The critical resonator vibration amplitude due to electrostatic nonlinearity is 36.0 nm at  $U_{dc} = 20$  V, which is well below the experimentally measured mechanical nonlinearity limit of 155 nm. Thus, the use of a simplified model that ignores the nonlinear mechanical effects is justified.

To focus on the resonator nonlinearity, a simple current controlled voltage source (CCVS) is used as an amplifier. To control the resonator vibration amplitude, the amplifier is made nonlinear and its output voltage is given by:

$$v = \frac{R}{a} \tanh(ai), \quad (39)$$

where  $R$  is the small signal transresistance,  $i$  is the input current, and  $a$  controls the amplifier saturation point. Thus, the amplifier gain and saturation point can be adjusted independently. At oscillator operation point, the amplifier saturates and provides transresistance  $R = R_m$ . By adjusting  $R$  and  $a$ , the amplifier linearity at the operation point can be adjusted. This is used to verify that

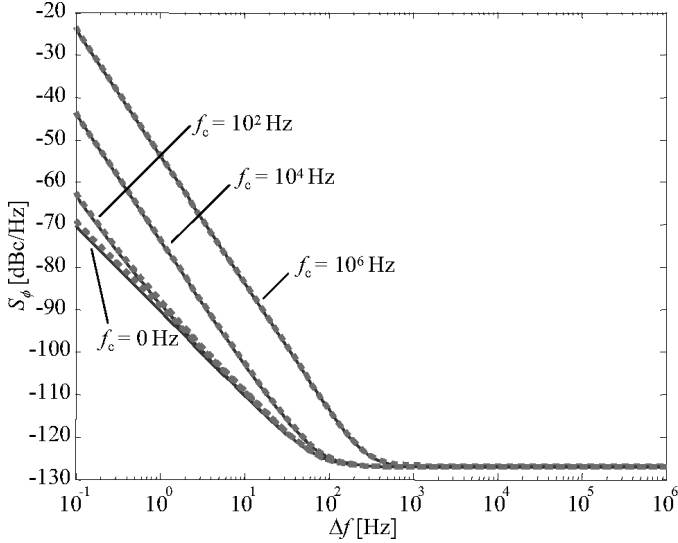


Fig. 9. Simulated (dotted line) and analytical (solid line) phase noise for different  $1/f$  corner frequencies  $f_c$  for the 13.2 MHz oscillator in Table I. As the  $1/f$ -noise is increased, the near-carrier phase noise slope changes from  $1/f^2$  to  $1/f^3$ .

resonator and not the amplifier is responsible for the aliasing. For added verification, the oscillator also was simulated with an ideal RLC resonator shown in Fig. 3. With the capacitive nonlinearity removed from the simulations, no aliased noise was observed in the simulations, showing that the resonator and not the amplifier is responsible for the noise up-mixing. We note that sufficiently linear amplifiers is well realizable in practice, although in commercial applications requirements for the circuit size and power consumption may lead a compromise of using a more non-linear amplifier.

Fig. 9 shows a comparison of simulated and analytical phase noise (37). The total noise at the resonator input is  $u_n = u_{n,t}(1 + f_c/\Delta f)$  where  $u_{n,t} = 10 \text{ nV}/\sqrt{\text{Hz}}$ . The resonator drive level is  $u_{ac} = 32 \text{ mV}$  or  $x/x_c = 0.28$ . Very good agreement is obtained between the theory and simulations. As the  $1/f$ -noise is increased, the near-carrier phase noise slope changes from  $1/f^2$  to  $1/f^3$ . At  $1/f$ -noise corner frequency greater than 10 kHz, no  $1/f^2$  region is observed.

The simulation time was less than 10 s with 2.2 GHz Pentium 4 computer (Intel Corporation, Santa Clara, CA) demonstrating the simulation speed advantage over the time domain simulations that are slow to converge for systems with a large quality factor.

## VI. EXPERIMENTAL VERIFICATION

To verify the analytical and simulation results on noise aliasing, phase noise in an oscillator shown in Fig. 10 was measured. For the phase noise measurement, Agilent 89640A vector signal analyzer (Agilent Technologies, Palo Alto, CA) was used in phase demodulation mode. As the dynamic range of the measurement instrument was only 120 dB,  $1/f$ -noise was added to the oscillator to bring

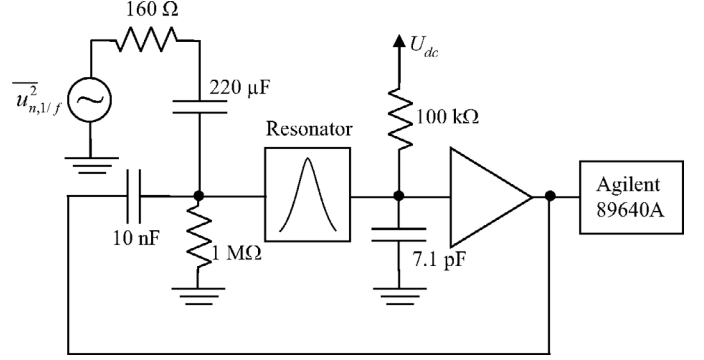


Fig. 10. Series mode micro-oscillator and the measurement set-up for phase noise. External noise source is used to verify the results on noise aliasing due to capacitive coupling.

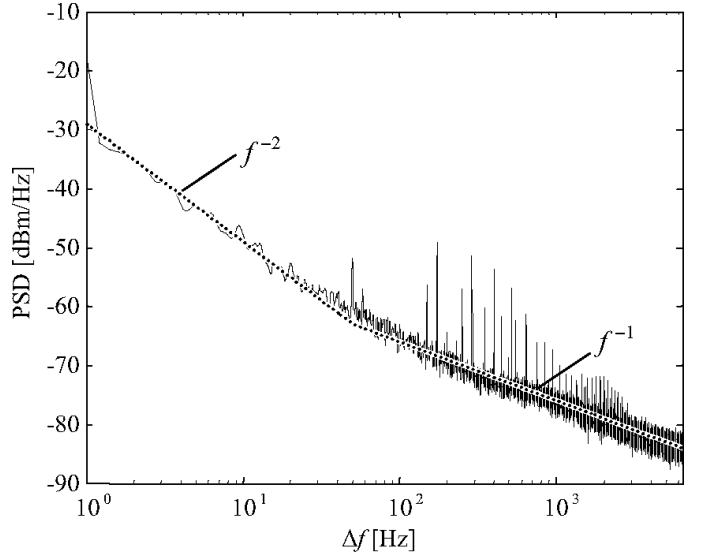


Fig. 11. Measured noise power spectral density for the external  $1/f$ -noise source. The solid line shows the noise model used in the simulations.

phase noise up to a measurable level. Using an external noise source also simplifies the measurements as the noise is well characterized, and the low-frequency noise dominates the oscillator phase noise. Also, as the  $1/f$ -noise source is connected to the resonator, it is effectively filtered and only the aliased noise reaches the amplifier. Thus, possible noise aliasing in the amplifier is effectively eliminated.

Fig. 11 shows the power spectral density (PSD) of the external  $1/f$ -noise source [20]. The solid line indicates the noise source model used in the simulations. The resonator used for the experiment is similar to the one described in Table I, except that  $Q = 26000$ ,  $d = 170 \text{ nm}$ , and  $U_{dc} = 15 \text{ V}$ . The low quality obtained with the narrow gap resonator in comparison to  $Q > 100000$  obtained with wide gap resonators is believed to be due to contaminants in the gap. In-situ anneal has been demonstrated to restore the quality factor [21].

Fig. 12 shows the simulated and measured phase noise at three different drive levels ( $u_{ac} = 54 \text{ mV}$ ,  $u_{ac} = 90 \text{ mV}$ ,

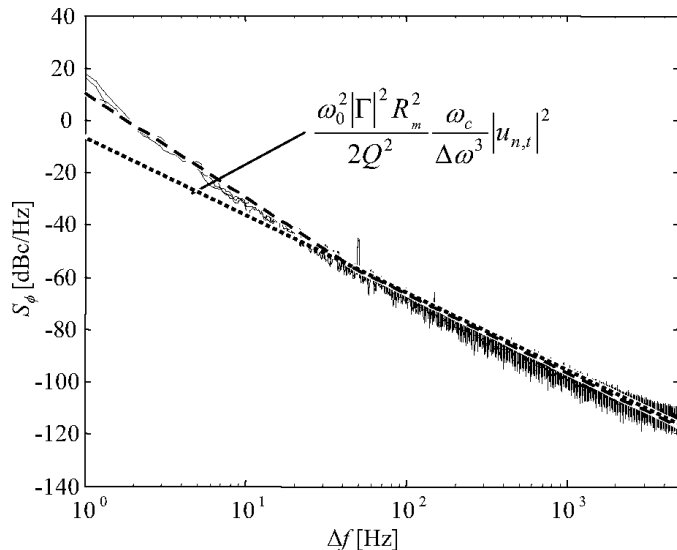


Fig. 12. Measured (solid lines) and simulated (dashed line) phase noise for a micro-oscillator at three different drive levels. Also shown is the analytical result (dotted line) for oscillator noise dominated by aliasing of  $1/f$ -noise.

and  $u_{ac} = 180$  mV or  $x/x_c = 0.070$ ,  $x/x_c = 0.118$ , and  $x/x_c = 0.235$ , respectively). Very good agreement is obtained between the simulations (dashed line) and experiment (solid lines). Moreover, as expected from (37), the near-carrier noise does not depend on the drive level, and the phase noises for the measured three drive levels are barely distinguishable. Also shown is the analytical noise given by (38) (dotted line) that agrees well in the  $1/f^3$ -region where the noise source has the  $1/f$  behavior. It should be mentioned that the noise performance in Fig. 12 does not reflect the true performance obtainable with microelectromechanical systems (MEMS), but the poor performance is a result of excessive  $1/f$ -noise injected in the oscillator for the ease of measurement.

## VII. DISCUSSION

Following the analysis in Section III, the noise aliasing factor can be reduced by:

- increasing the electrode gap  $d$ ,
- decreasing the quality factor  $Q$ ,
- increasing the stiffness  $k$ ,
- lowering the bias voltage  $U_{dc}$ ,
- use of linear transducer capacitance  $C(x) = C_0(1 + x/d)$ ,

All these methods also will increase the motional impedance  $R_m$ . Large  $R_m$  makes the realization of good oscillator more difficult and requires larger amplifier gain, which in turn amplifies the noise as seen in (38). Larger gap and bias voltage could be used to reduce aliasing while keeping the electromechanical transduction constant; but, unfortunately, the large bias voltages are not preferred due to technological reasons. Linear electrodes such as comb drives appear attractive for reducing the aliasing but also

yield weaker electromechanical transduction than parallel plate electrodes. Grounded resonator with separate drive and pick-up electrodes can be used to eliminate the direct current aliasing path (Section III-A) but it does not eliminate the force aliasing (Section III-B) that is the dominant noise aliasing mechanisms. As no panacea appear for removing the aliasing, effort should be focused on reducing the low-frequency noise. Low-noise loop amplifiers together with high-pass filters may be effective in reducing the noise appearing at the resonator input, thus lowering the oscillator near-carrier noise.

This paper has analyzed the noise aliasing in a resonator. In some practical oscillator implementations the noise aliasing in the amplifier also may contribute to the near-carrier noise, and both the amplifier and resonator nonlinearity needs to be accounted for an accurate model of oscillator phase noise. Although this is beyond the scope of this paper's focus on resonator nonlinearity, the design insights and analysis tools presented are applicable for possible cases of combined amplifier and resonator nonlinearity.

## VIII. CONCLUSIONS

The capacitive transduction commonly used in microresonators is shown to result in the aliasing of  $1/f$ -noise to carrier side-bands and can significantly affect the oscillator phase noise performance. Consequently the near-carrier noise is expected to be worse for capacitively actuated resonators than for similar piezoelectrically actuated resonators. A detailed analysis of the noise-mixing mechanisms was carried out, and the capacitive force nonlinearity was found to be the dominant up-mixing mechanism in electrostatic transduction. An analytical model of oscillator phase noise model was developed and verified with simulations. The analytical model and simulations were compared to the experimentally measured micro-oscillator phase noise, and excellent agreement with the theory and experimental results was obtained. Thus, the analytical and simulation methods presented can be used for quantitative prediction of noise in micro-oscillators.

## ACKNOWLEDGMENT

We thank Jaakko Juntunen at Aplac Solutions, Inc., for technical support and Jyrki Kiihamäki for sample fabrication. We acknowledge financing from European Union (Mimosa-FR-6).

## REFERENCES

- [1] T. Mattila, J. Kiihamäki, T. Lamminmäki, O. Jaakkola, P. Rantakari, A. Oja, H. Seppä, H. Kattelus, and I. Tittonen, "12 MHz micromechanical bulk acoustic mode oscillator," *Sens. Actuators A*, vol. 101, no. 1-2, pp. 1-9, Sep. 2002.

- [2] V. Kaajakari, T. Mattila, A. Oja, J. Kiihamäki, H. Kattelus, M. Koskenuori, P. Rantakari, I. Tittonen, and H. Seppä, "Square-extensional mode single-crystal silicon micromechanical RF-resonator," in *Proc. Transducers'04, 12th Int. Conf. Solid-State Sens. Actuators*, 2004, pp. 951–954.
- [3] V. Kaajakari, T. Mattila, J. Kiihamäki, H. Kattelus, A. Oja, and H. Seppä, "Nonlinearities in single-crystal silicon micromechanical resonators," in *Proc. Transducers'04, 12th Int. Conf. Solid-State Sens. Actuators*, 2004, pp. 1574–1577.
- [4] V. Kaajakari, T. Mattila, A. Oja, and H. Seppä, "Nonlinear limits for single-crystal silicon microresonators," *J. Microelectromech. Syst.*, vol. 13, no. 5, pp. 715–724, Oct. 2004.
- [5] V. Kaajakari, T. Mattila, A. Oja, J. Kiihamäki, and H. Seppä, "Square-extensional mode single-crystal silicon micromechanical resonator for low phase noise oscillator applications," *IEEE Electron. Device Lett.*, vol. 25, no. 4, pp. 173–175, Apr. 2004.
- [6] Y.-W. Lin, S. Lee, S.-S. Li, Y. Xie, Z. Ren, and C. T.-C. Nguyen, "Series-resonant VHF micromechanical resonator reference oscillators," *IEEE J. Solid-State Circuits*, vol. 39, no. 12, pp. 2477–2491, Dec. 2004.
- [7] G. Sauvage, "Phase noise in oscillators: A mathematical analysis of Leeson's model," *IEEE Trans. Instrum. Meas.*, vol. 26, no. 4, pp. 408–410, Dec. 1977.
- [8] W. Robins, *Phase Noise in Signal Sources (Theory and Applications)*. ser. IEE Telecommunication Series 9. London: Peter Peregrinus, 1982.
- [9] B. Razavi, "A study of phase noise in CMOS oscillators," *IEEE J. Solid-State Circuits*, vol. 31, no. 3, pp. 331–343, Mar. 1996.
- [10] T. Lee, *The Design of CMOS Radio-Frequency Integrated Circuits*. Cambridge: Cambridge Univ. Press, 1998.
- [11] T. H. Lee and A. Hajimiri, "Oscillator phase noise: A tutorial," *IEEE J. Solid-State Circuits*, vol. 35, no. 3, pp. 326–336, Mar. 2000.
- [12] H. Tilmans, "Equivalent circuit representation of electromechanical transducers: I. Lumped-parameter systems," *J. Microelectromech. Syst.*, vol. 6, no. 1, pp. 157–176, Mar. 1996.
- [13] V. Kaajakari, T. Mattila, A. Lipsanen, and A. Oja, "Nonlinear mechanical effects in silicon longitudinal mode beam resonators," *Sens. Actuators A*, vol. 120, no. 1, pp. 64–70, Apr. 2005.
- [14] T. Veijola and T. Mattila, "Modeling of nonlinear micromechanical resonators and their simulation with the harmonic-balance method," *Int. J. RF Microwave Comput. Aided Eng.*, vol. 11, no. 5, pp. 310–321, Sep. 2001.
- [15] L. D. Landau and E. M. Lifshitz, *Mechanics*. Oxford: Butterworth-Heinemann, 1999.
- [16] C. T.-C. Nguyen and R. T. Howe, "CMOS micromechanical resonator oscillator," in *Proc. IEEE Int. Electron Devices Meeting*, 1993, pp. 199–202.
- [17] B. Razavi, *RF Microelectronics*. Englewood Cliffs, NJ: Prentice-Hall, 1998.
- [18] J. R. Vig and Y. Kim, "Noise in microelectromechanical system resonators," *IEEE Trans. Ultrason., Ferroelect., Freq. Contr.*, vol. 46, no. 6, pp. 1558–1565, Nov. 1999.
- [19] H. Jokinen, "Computation of the steady-state solution of nonlinear circuits with time-domain and large-signal–small-signal analysis methods," Ph.D. dissertation, Helsinki University of Technology, Helsinki, Finland, 1997.
- [20] J. Barnes and J. S. Jarvis, "Efficient numerical and analog modeling of flicker noise processes," Washington, DC: National Bureau of Standards, Technical Report 604, 1971.
- [21] A.-C. Wong, H. Ding, and C. T.-C. Nguyen, "Micromechanical mixer+filters," in *IEEE Int. Electron Devices Meeting*, 1998, pp. 471–474.



**Ville Kaajakari** received his M.S. and Ph.D. degrees in electrical and computer engineering from University of Wisconsin-Madison in 2001 and 2002, respectively. He is currently Senior Research Scientist at VTT Information Technology, Finland, where his research interest is RF-MEMS.



**Jukka K. Koskinen** is working towards the M.Sc. degree in electrical and computer engineering at Helsinki University of Technology, Helsinki, Finland. He is currently employed at VTT Information Technology, Finland, where his research interest is RF-MEMS and integrated circuits.



**Tomi Mattila** received his M.Sc. and Dr.Tech. degrees from the Department of Technical Physics at Helsinki University of Technology in 1994 and 1997, respectively. Since 1999 he has been working as Senior Research Scientist at VTT. His current research interests concentrate on micromechanical RF-devices.